Synergistic Regulation of Bidirectional Conversion of LiPSs and Li_2S Using Anthraquinone as a Redox Mediator

Huijuan You, Zining Wang, Xuyun Wang,* Jianwei Ren,* Hui Wang, and Rongfang Wang*

ABSTRACT: Lithium−sulfur (Li−S) batteries are strong contenders as energy storage options in the next-generation, primarily because of their potential for delivering high energy densities. Nonetheless, their widespread commercialization faces several obstacles, including sluggish sulfur redox kinetics, the insulating properties of the Li_2S discharge product, and significant reaction energy barriers. In this work, anthraquinone (AQ) was introduced as a redox mediator and incorporated onto Co-doped carbon materials through $\pi-\pi$ interactions. The results showed that synergistic effect between AQ and Co atoms facilitated the bidirectional conversion of lithium polysulfides (LiPSs) and Li_2S. During charging, AQ lowered the reaction energy barrier for Li_2S oxidation and thereby enhanced the reversibility of sulfur redox reactions. Density functional theory (DFT) calculations showed that AQ-Li_2S_x exhibits a lower energy for the lowest unoccupied molecular orbital (LUMO) and a higher energy for the highest occupied molecular orbital (HOMO). Experimental results demonstrated that an impressive initial discharge specific capacity of 1290 mAh g^{-1} was achieved by the fabricated S@AQ/Co−N−C electrode at 0.1 C. After 600 cycles at 1 C, it retained 64% of this capacity and exhibited a minimal 0.06% capacity decay rate per cycle.

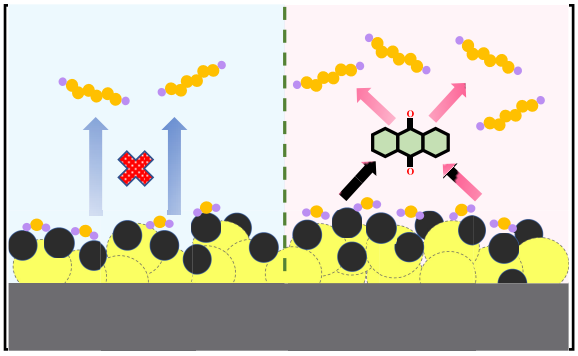

KEYWORDS: *Lithium−sulfur batteries, Redox mediators, Anthraquinone, Redox reaction kinetics, Positive synergistic effect*

1. INTRODUCTION

The swift growth of portable electronics, electric vehicles, digitalization, and smart grid applications has heightened an demand for high energy density and cost-effective energy storage solutions.[1,2] With a high theoretical energy density of up to 2600 Wh kg^{-1}, lithium−sulfur (Li−S) batteries have emerged as competitive for next-generation energy storage options.[3,4] The sulfur redox reaction involves a complex multiphase dissolution−deposition process, beginning with solid S_8 transitioning to soluble lithium polysulfides (LiPSs) and ultimately forming insoluble Li_2S_2/Li_2S. This reaction provides a high theoretical specific capacity of 1675 mAh g^{-1}.[5−8] Sulfur as a cathode material also offers significant advantages, including its natural abundance, environmental compatibility, and low cost.[9] However, the electrochemical behavior of sulfur in Li−S systems entails multielectron reactions and solid−liquid−solid phase changes, presenting challenges such as the uncontrolled shuttling of soluble LiPSs. This shuttling effect leads to rapid capacity loss of the sulfur cathode and severe corrosion of the lithium anode, thus, limiting the practical viability of Li−S batteries. Addressing these issues is critical to enhancing the performance of Li−S batteries through the effective management of LiPS shuttling and conversion.[10−13] Several strategies have been investigated in the literature, including the use of functional separators to reduce polysulfide migration,[14−18] the incorporation of micro/nano host materials to immobilize or adsorb polysulfides,[19−22] and the modification of electrolytes or electrodes with additives to protect the cathode and anode.[23,24] While several host materials have been investigated for their ability to inhibit shuttling through physical or chemical confinement of soluble LiPSs,[25−28] the slow conversion of solid Li_2S and saturation of host material surfaces with adsorbed LiPSs increase the concentration of soluble LiPSs in the electrolyte.[29,30] These issues compromise the efficacy of applied strategies in limiting LiPSs shuttling over long-term cycling, particularly when the sulfur loading on cathodes is high. Meanwhile, poor kinetic performance during the liquid−solid phase transitions further impedes the reversibility of sulfur cathodes.[31] Consequently, novel approaches are required to facilitate the efficient conversion between Li_2S and LiPSs and thereby improve the overall performance of Li−S batteries.

Solid mediators like metal nitrides,[32,33] oxides,[34−37] sulfides,[38,39] and their heterostructures are capable of electrochemically catalyzing the LiPSs conversion and eventually enhancing the overall Li−S battery performance. However, these metal-based catalysts primarily accelerate electron transfer and do not effectively reduce the formation of "dead sulfur".[40] In contrast, the introduction of redox mediators (RMs) has the potential to provide an additional redox pathway (ARP). RMs have been utilized in secondary batteries, including Li−O_2 batteries,[41−43] Na/Li-ion batteries,[44] and Li−S batteries.[45−47] The conversion of LiPSs was promotedby RMs via a two-step mechanism that includes both electrochemical and chemical reactions. In the charging process, while the oxidized form of RMs (RMox) oxidizes Li_2S to LiPSs chemically, RMox is reduced to its reduced form (RMred). RMred is then electrochemically oxidized back to RMox after providing electrons to the current collector. This process reduces the formation of "dead sulfur" and maintains more active sulfur by transferring electrons between the current collector and the insulating Li_2S.[48] For example, Peng et al.[49] employed 5,7,12,14-pentacenetetrone (PT) as a redox mediator to improve the reduction of LiPSs to Li_2S. The resulting electrode demonstrated a discharge specific capacity of 933 mAh g^{-1} at 0.1 C, with a low electrolyte-to-sulfur ratio (E/S) of 5 μL mg^{-1} and a high sulfur loading of 4 mg cm^{-2}. 1,4-Difluoroanthraquinone (DFAQ) was utilized by Zhang et al.[50] as a bifunctional additive to create a solid electrolyte interphase (SEI) layer that not only protected the lithium anode but also acted as a redox mediator. This enhanced the conversion of LiPSs to Li_2S and mitigated the shuttle effect. As a result, a discharge specific capacity of 1022.3 mAh $g^{-1}$was achieved by the Li−S battery with DFAQ addition after 300 cycles at 0.1 C. Despite these advancements, most previous studies focused on promoting the reduction of LiPSs to Li_2S, and limited attention has been given to activate Li_2S and lower the reaction energy barrier. Within Li−S batteries, the transformation of LiPSs into Li_2S occurs spontaneously, while the reverse reaction of oxidizing Li_2S to LiPSs is a nonspontaneous process. More specifically, enhancing the conversion from Li_2S to LiPSs is crucial for improving battery performance, and overcoming the high reaction energy barrier during this process remains a critical challenge. The soluble-type quinone-based RM (AQT) was evaluated by Gao et al.[48] as a redox mediator. The findings indicated that AQT activated Li_2S at an oxidation potential exceeding the equilibrium potential of Li_2S, which is 2.15 V. The evolution of sulfur species provides an ARP to promote the oxidation of Li_2S to LiPSs. The reversible oxidation and reduction of RMs during electrochemical cycling is crucial for the performance of Li−S battery-based energy storage systems.[51] In lithium-ion batteries (LIBs), RMs promote oxidation and reduction reversibly at an oxidation potential just above the fully charged voltage. They provide extra charge and serve as chemical protectors against overcharge in liquid electrolytes to enhance battery safety.[52] Additionally, RMs may be incorporated as additives in liquid electrolytes to improve charge transfer at the electrode−electrolyte interface.[53] Thereby, they can activate the insulating discharge products like lithium oxide or lithium peroxide[54,55] and Li_2S_2/Li_2S.[56−58] Notably, RMs are usually small molecules that easily solute into liquid-phase electrolytes and then move freely. This often leads to potential reactions with lithium metal and causes lithium anode corrosion.[59] Therefore, anchoring organic molecules onto the cathode can effectively reduce the corrosion of the lithium anode.

In this work, anthraquinone (AQ) was loaded onto a Co−N-doped carbon substrate via $\pi-\pi$ interactions, and the resulting composite was utilized in Li−S battery cathodes. As detailed in our previous work,[60] Co atoms adsorbed LiPSs and promoted their catalytic conversion during discharge by forming Co−S bonds with LiPSs. During charging, AQ acted as a RM to lower the oxidation energy barrier of Li_2S, activate the insulating Li_2S, and provide an ARP to enhance the utilization of active sulfur. The combined effect of AQ and cobalt (Co) enhanced the bidirectional conversion of the LiPSs. Because of that, the optimized S@AQ/Co−N−C electrode sample achieved a 12% improvement in the initial discharge specific capacity at 0.1 C. At 1 C, it demonstrated 64% capacity retention after 600 cycles, with a low-capacity decay rate of just 0.06% per cycle. This study highlights the effectiveness of AQ as a redox mediator, working synergistically with metallic Co to enable high-performance Li−S batteries.

2. EXPERIMENTAL SECTION

2.1. Preparation of Co−N−C Sample. In a typical process, 1 g of peptone and 0.03 mmol of $Co(NO_3)_2{\cdot}6H_2O$ were dissolved together in 2 mL of deionized water, and the mixture was ultrasonicated for 5−10 min until fully dissolved. The solution was then frozen for 12 h in ice blocks, which were subsequently freeze-dried for 12 h. The dried material was combined with NaCl (10 g) and subjected to a ball milling operation at 550 rpm for 3 h. The milled mixture was transferred to a tube furnace, which was heated up gradually to 900 °C at a rate of 5 °C/min under an N_2 atmosphere and maintained at this temperature for 1 h for high-temperature pyrolysis. After cooling, the final product was collected and washed to remove residues before being dried in an oven at 60 °C.

2.2. Preparation of AQ/Co−N−C Sample. Typically, Co−N−C (60 mg) was dispersed in a 0.05 mM AQ solution (20 mL), and the mixture was stirred for 30 min using a magnetic stirrer. The product was then centrifuged and dried in an oven at 60 °C for 6 h.

2.3. Preparation of S@Co−N−C and S@AQ/Co−N−C Samples. The Co−N−C and AQ/Co−N−C samples prepared in Steps 2.1 and 2.2, respectively, were each individually mixed with sublimed sulfur at a mass ratio of 2:3. The mixture underwent grilling for 30 min before being transferred into a reactor within an argon-filled glovebox. The reactor was subsequently placed in a preheated oven at 155 °C for 12 h to produce the S@Co−N−C and S@AQ/Co−N−C samples.

2.4. Preparation of Li_2S_6 Solutions. Li_2S and sublimed sulfur were combined in a molar ratio of 1:5 and added to a mixed solvent of ethylene glycol dimethyl ether and 1,3-dioxolane (DME/DOL, v/v = 1:1). The mixture was heated to 60 °C and stirred for 24 h to yield the 0.2 M Li_2S_6 solution. Similarly, a 5 mM Li_2S_6 solution was prepared by using the same procedure.

2.5. Adsorption Experiments. In a typical experiment, 5 mg of Co−N−C and AQ/Co−N−C samples was separately added to a 5 mM Li_2S_6 solution (5 mL). The mixtures were allowed to stand for 2 h to observe any color changes.

2.6. Physical Characterization. In situ synchrotron radiation measurements were performed at the Shanghai Synchrotron Radiation Facility using the BL08U1A beamline. X-ray Diffraction (XRD) analysis was performed on an X-ray diffractometer (Rigaku MiniFlex 600, Japan) with a scanning rate of 10°/min across a 2θ range of 10−80°. Transmission electron microscopy (TEM) was performed using a JEOL JEM-2000FX transmission electron microscope (Japan), also with imaging across different regions. Scanning electron microscopy (SEM) imaging was conducted with a Carl Zeiss Ultra Plus scanning electron microscope (Germany), capturing various regions of the sample. UV−vis spectroscopy measurements

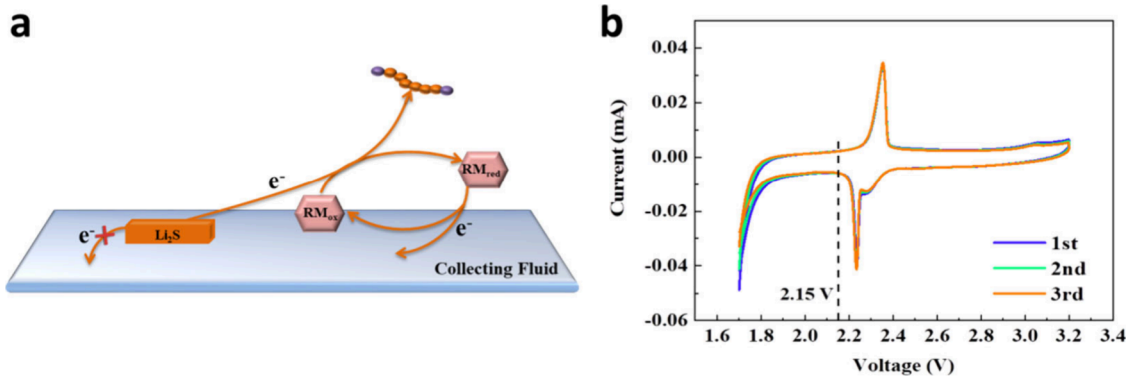

Figure 1. (a) Schematic illustration showing the function of a redox mediator in enhancing the performance of Li−S batteries. (b) Cyclic voltammetry (CV) curve of the LillAQ system.

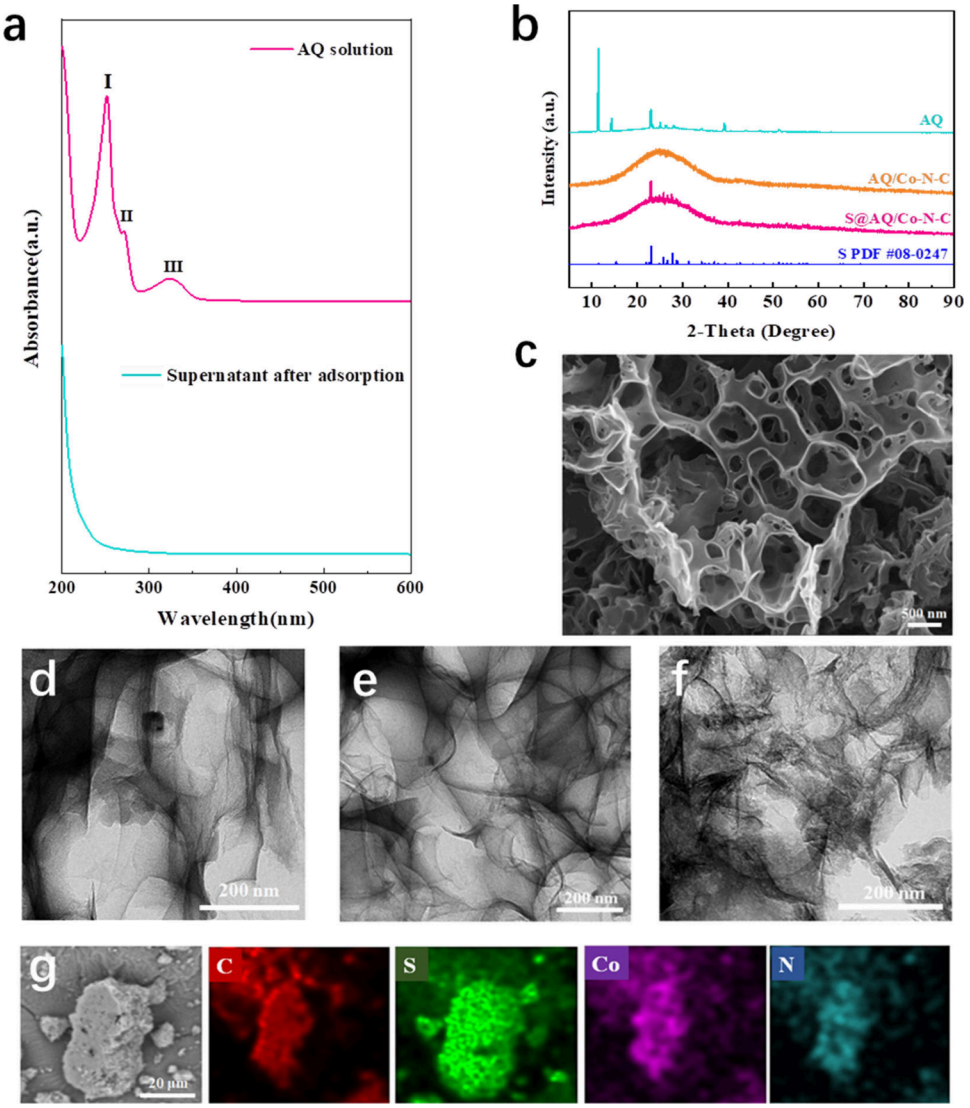

Figure 2. (a) UV absorption spectra of the AQ solution and the supernatant after adsorption by carbon material. (b) XRD spectra of AQ, AQ/Co−N−C, and S@AQ/Co−N−C samples. (c) SEM image of the Co−N−C sample. TEM images of the samples: (d) Co−N−C, (e) AQ/Co−N−C, and (f) S@AQ/Co−N−C. (g) Elemental mapping of C, S, Co, and N in the S@AQ/Co−N−C sample.

were obtained with a UV-5800 PC UV−visible spectrophotometer, covering a wavelength range from 200 to 400 nm.

2.7. Evaluation of Electrochemical Performance. Typically, S@AQ/Co−N−C, conductive carbon black Super P, and binder PVDF in a mass ratio of 7:2:1 was dissolved in NMP under continuous stirring. The resulting slurry was then coated onto an aluminum foil current collector and dried for 12 h at 60 °C to form the sulfur cathode. The assembling process of the coin cell was carried out in an argon-filled glovebox, using the 1.0 M LiTFSI solution in DME/DOL (volume ratio = 1:1) with 1.0% $LiNO_3$ as the electrolyte,

Celgard 2400 (diameter: 16 mm) as the separator, metallic lithium (diameter, 15.6 mm; thickness, 0.45 mm) as the anode, and a CR2032 stainless steel battery casing. Unless otherwise noted, the mass loading of sulfur in the electrode was approximately 1.2−1.4 mg cm^{-2} (diameter: 12 mm), and the electrolyte-to-sulfur (E/S) ratio was about 40 μL mg^{-1}. For the symmetric cell, the ingredients of AQ/Co−N−C, PVDF, and Super P in a mass ratio of 8:1:1 were mixed and dissolved in NMP, and the obtained slurry was coated onto carbon paper, which was then dried at 60 °C. In assembling the symmetric cell, a 0.2 M Li_2S_6 solution (60 μL) was used as the electrolyte.

The discharge and constant current charge tests were carried out on a Newway battery system, and the voltage range was set between 1.7 and 2.8 V. The electrochemical impedance spectroscopy (EIS) measurements and cyclic voltammetry (CV) were done on an electrochemical analyzer (CHI 650D). The EIS tests covered the frequency range of 100 kHz−10 mHz. All of those experiments were conducted at room temperature. For the CV measurements, a scanning rate of 0.1 mV s^{-1} was applied within the voltage window of 1.7−2.8 V. The peak current observed at scanning rates between 0.1 and 0.5 mV s^{-1} was analyzed using the Randles−Sevcik equation.

$$I_P = (2.69 \times 10^5) \times n^{1.5} \times A \times D_{Li}^{0.5} \times C_{Li} \times v^{0.5}$$

In this equation, I_P represents the peak current (A), n denotes the number of electrons involved in the reaction (n = 2), A represents the electrode area, D_{Li} is the diffusion coefficient of Li^+, C_{Li} represents the concentration of Li^+ in the electrolyte, and v denotes the potential scan rate.

2.8. Theoretical Calculation. Calculations were conducted using the B3LYP density functional method in the Gaussian 09 program with the 6-31G(D) basis set. Dispersion corrections were applied using the empirical keyword (em = gd3bj). All molecular structures were optimized and confirmed to have no imaginary frequencies. The lowest unoccupied molecular orbital (LUMO), highest occupied molecular orbital (HOMO), and electrostatic surface potential (ESP) were computed and visualized by using Multiwfn and Visual Molecular Dynamics (VMD).

3. RESULTS AND DISCUSSIONS

Figure 1a presents a schematic representation that highlights the function of AQ as a redox mediator while controlling the transformation of Li_2S into LiPSs. Since Li_2S is insulating, portions of Li_2S not in direct contact with the current collector cannot directly transfer electrons. This prevents them from converting to LiPSs and results in the formation of "dead sulfur". After the addition of AQ, it acts as a mediator, providing an additional pathway for electron transfer. With a higher oxidation potential than Li_2S, AQ oxidizes Li_2S into LiPSs while being reduced itself. The reduced AQ then transfers electrons to the current collector and returns to its oxidized state. This cyclic process facilitates the conversion of insulating Li_2S into LiPSs and reduces the formation of "dead sulfur". Figure 1b illustrates that the oxidation potential of AQ exceeds the equilibrium potential of 2.15 V from Li_2S.[56] The reaction equations are as follows: eq 1 shows the oxidation of Li_2S to LiPSs, eq 2 depicts the reduction of AQ as it gains electrons, and eq 3 represents the overall role of AQ in the sulfur redox reaction as a redox mediator.

$Li_2S \rightarrow Li_2S_x (2 < x \leq 8)$:

$$xLi_2S - (2x-2)e^- \rightarrow Li_2S_x + (2x-2)Li^+ \quad (1)$$

$$AQ + e^- \rightarrow AQ^- \quad (2)$$

$$(2x-2)AQ + xLi_2S \rightarrow Li_2S_x + (2x-2)AQ^- + (2x-2)Li^+ \quad (3)$$

The Gibbs free energy (ΔG) calculation formula in the context of electrochemical reactions is as follows:

$$E = \varphi_+ - \varphi_- = \varphi_{AQ/AQ^-} - \varphi_{Li_2S_x/Li_2S} > 0 \quad (4)$$

$$\Delta G = -nFE < 0 \quad (5)$$

Here, x denotes the number of molecules, EEE refers to the potential difference, E represents the number of electrons transferred, and F stands for the Faraday constant (F = 96500 C mol^{-1}). It was further demonstrated through calculations that AQ as a redox mediator can oxidize Li_2S and reduce the formation of "dead sulfur".

The molecular structure of AQ and its interaction with carbon materials were analyzed by using UV absorption spectroscopy. Figure 2a depicts three UV absorption distinct peaks from the AQ solution exhibits three. Both peak I at 252 nm and peak III at 325 nm are associated with the molecular structure of benzene ring, while peak II at 273 nm is attributed to the structure of carbonyl group.[61] The carbon support used in this work is a cobalt-loaded and nitrogen-doped 3D carbon network. In the meantime, upon dispersion of the carbon material in the AQ solution, the UV absorption peaks of AQ are notably reduced or completely vanish due to adsorption by the carbon material. This indicates that the π-structure of the graphite layers in the carbon material interacts with the π-structure of AQ through $\pi-\pi$ interactions, which yield the AQ/Co−N−C composite. The AQ/Co−N−C sample was immersed in electrolyte for 7 days prior to UV spectroscopy analysis. As observed in Supporting Information (SI), Figure S1, the UV spectrum of the electrolyte containing dispersed AQ/Co−N−C matches that of the pure electrolyte. This implies that AQ did not dissolve in the electrolyte and remained stably adsorbed on Co−N−C through $\pi-\pi$ interactions. For comparison, the porous Co−N−C material was synthesized to serve as the carbon substrate. Consequetically, the S@Co−N−C and S@AQ/Co−N−C electrode samples were prepared by following the sulfur loading via a melt diffusion method. The crystal structures of these samples were characterized by using X-ray diffraction (XRD). As shown in Figure 2b, AQ exhibits good crystallinity, but no AQ diffraction peaks are detected in AQ/Co−N−C sample due to the good dispersion of AQ on the carbon material. Except for the diffraction peaks from the carbon substrate, the XRD pattern of the S@AQ/Co−N−C sample reveals several peaks corresponding to the characteristic diffraction patterns of orthorhombic crystalline sulfur (JCPDS card no. 08-0247). This indicates that elemental sulfur is distributed uniformly within the carbon substrate.[62] The morphology of the materials was analyzed by using scanning electron microscopy (SEM). As illustrated in Figure 2c, the synthesized Co−N−C forms a three-dimensional (3D) structure of carbon network. This observation is further supported by the transmission electron microscopy (TEM) images shown in Figure 2d. As seen, the TEM image of the AQ/Co−N−C sample (Figure 2e) shows a smooth and uniform carbon network surface with no aggregation, which indicates that AQ is evenly distributed on the carbon material surface. The TEM image of the S@AQ/Co−N−C sample in Figure 2f reveals an intact carbon network structure after loading of sulfur, and there is no significant sulfur particle aggregation observed. This suggests

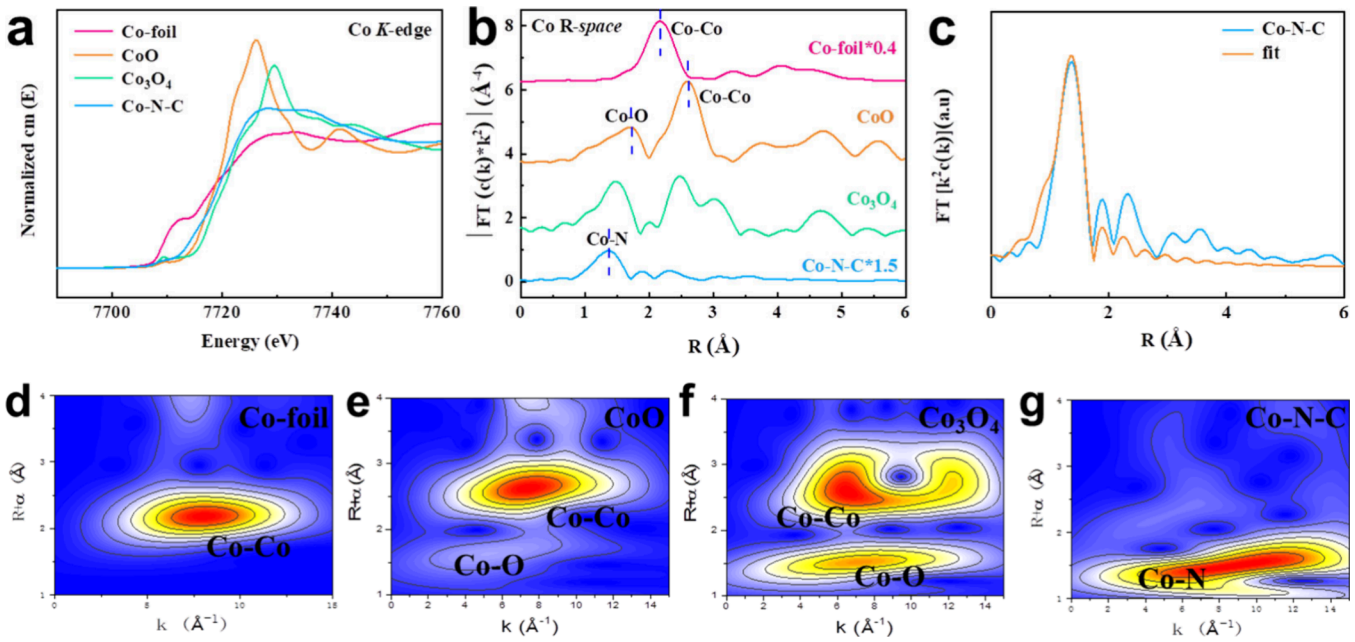

Figure 3. (a) Co K-edge XANES, (b) FT-EXAFS of Co K-edge at R space, and (c) EXAFS fitting curve of the Co−N−C structure. (d−g) WT-EXAFS of the Co K-edge for Co−N−C, along with standard CoO, Co_3O_4, and Co foil samples.

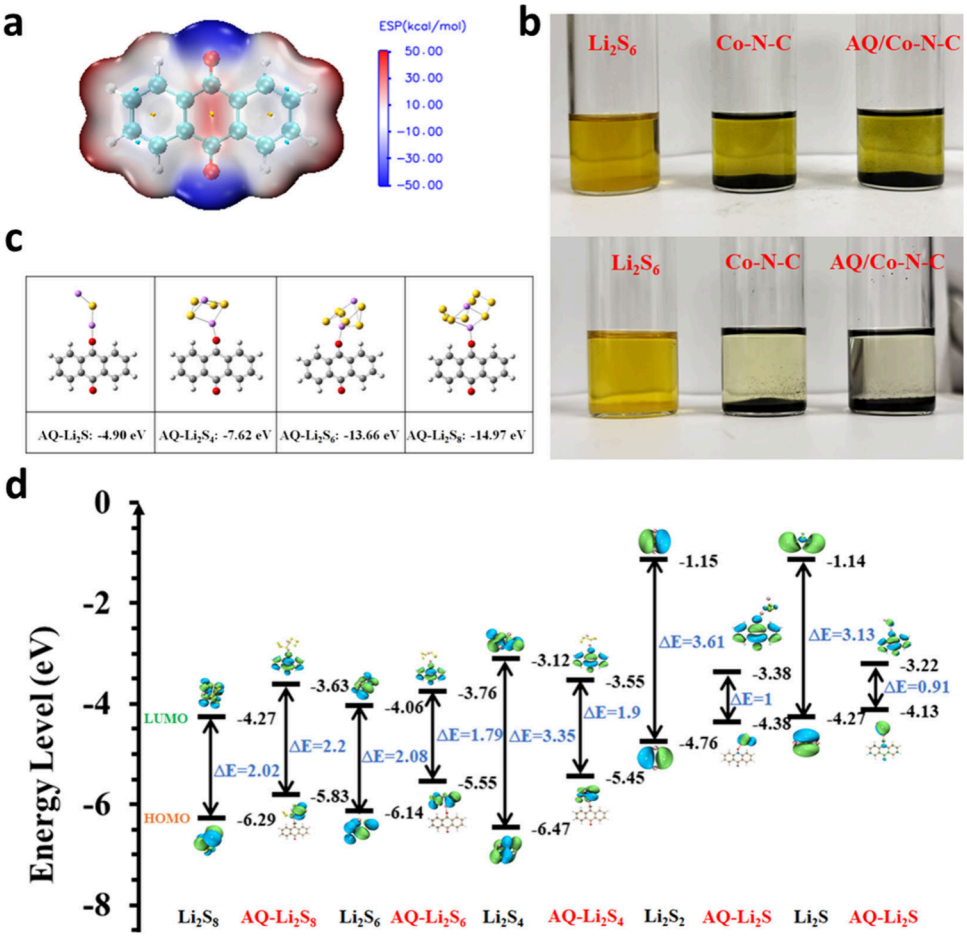

Figure 4. (a) Electrostatic potential map of the AQ molecule. (b) Static adsorption test images of Li_2S_6 solution after the addition of Co−N−C or AQ/Co−N−C sample, individually. (c) Adsorption configuration of AQ-Li_2S_x and its binding energy. (d) The molecular orbital energy levels of Li_2S_x and AQ-Li_2S_x.

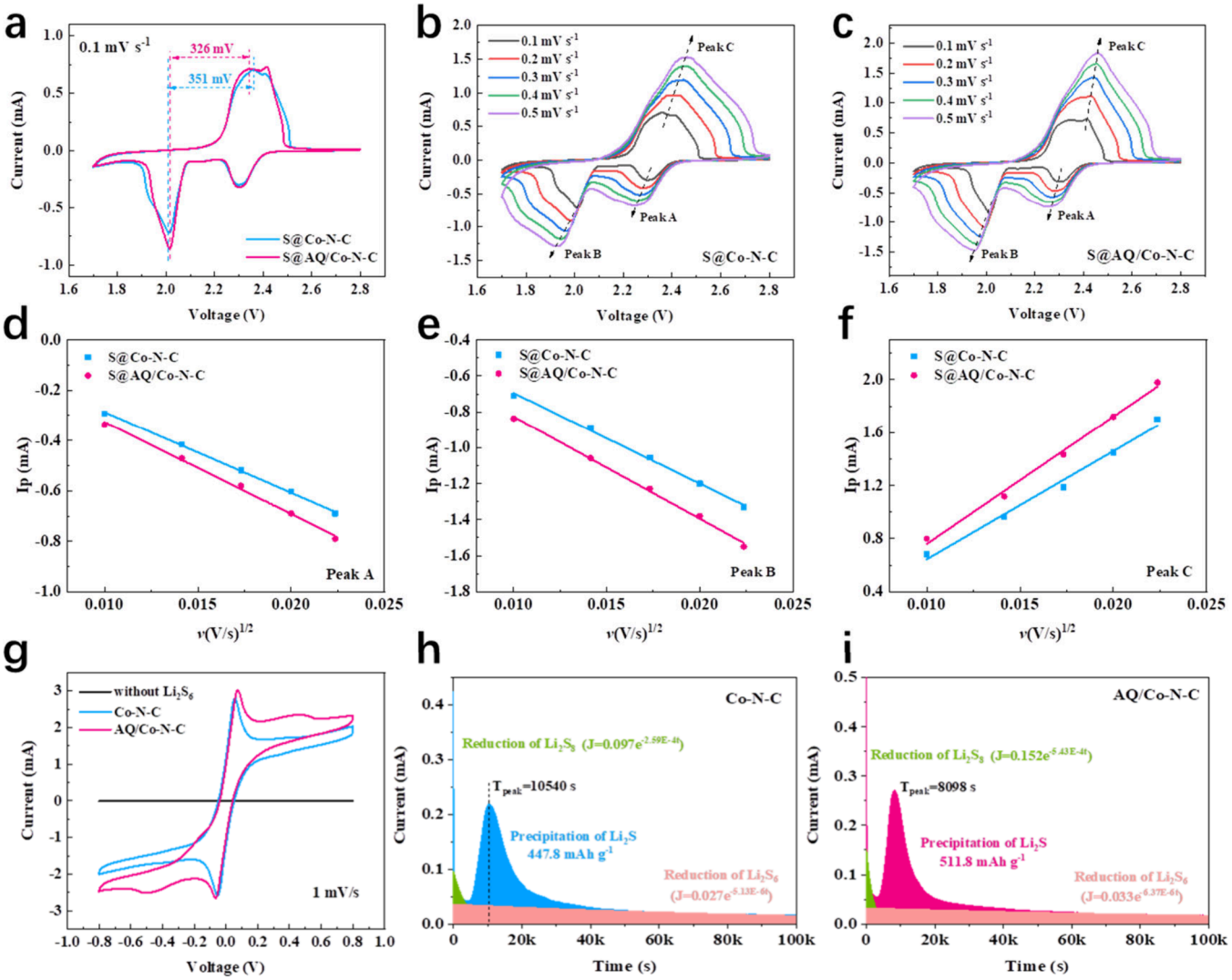

Figure 5. CV curves for the (a) S@Co−N−C and S@AQ/Co−N−C samples were recorded at a scan rate of 0.1 mV s^{-1}. CV curves of the (b) S@Co−N−C and (c) S@AQ/Co−N−C samples scanned at 0.1−0.5 mV s^{-1}, respectively. The peak currents and their corresponding linear fits for: (d) peak A, (e) peak B, and (f) peak C. (g) CV curves of two Co−N−C and AQ/Co−N−C samples in a Li_2S_6 solution at a scan rate of 1 mV s^{-1}. Deposition curves of Li_2S_8 on the sample surfaces for (h) the Co−N−C electrode at 2.05 V and (i) the AQ/Co−N−C electrode at 2.05 V.

that sulfur is uniformly dispersed within the carbon matrix. Meanwhile, the elemental mapping of the S@AQ/Co−N−C sample in Figure 2g displays an overlapping distribution of the S and C elements. This further validates the uniform distribution of sulfur within the carbon support. To identify the optimal AQ loading, the discharge specific capacities of S@AQ/Co−N−C electrodes with different AQ concentrations were evaluated at a current density of 0.2 C. As observed in SI, Figure S2, all batteries with AQ exhibited higher specific capacities compared to those without AQ. This implies that the addition of AQ effectively improves sulfur utilization. In contrast, the one with a 0.05 mM AQ loading achieved the best electrochemical performance. This is mainly due to AQ, as an organic small molecule, having both redox activity and the capability to function as a redox mediator, which aids in conversing LiPSs and thus improves sulfur utilization. However, it is insufficient to adsorb polysulfides effectively when the amount of AQ is too low. Conversely, excessive AQ can aggregate, obscure some of the Co active sites, and eventually reduce the electrocatalytic performance. Therefore, the sample with a 0.05 mM AQ loading was selected for further electrochemical tests.

X-ray absorption fine structure (XAFS) analysis is employed to examine the electronic structure and coordination environment of the sample.[63−65] As depicted in Figure 3a, the X-ray absorption near edge structure (XANES) spectrum of the Co−N−C sample lies between those of Co-foil and Co_3O_4. This suggests that, within the Co−N−C substrate, the oxidation state of Co sits between 0 (Co-foil) and +2 (CoO). The fitting results shown in SI, Figure S3, further supports this finding. Figure 3b shows the spectrum of Fourier transform extended X-ray absorption fine structure (FT-EXAFS) from the Co−N−C sample. The distinct peak around 1.38 Å is attributed to Co−N bonds. This suggests the successful doping of Co and N into the carbon matrix, forming stable Co−N bonds. In contrast, the absence of detectable Co−Co or Co−O peaks suggests that Co clusters or oxides are not present within the Co−N−C structure. These results confirm the successful preparation of a Co/N dual-doped Co−N−C porous carbon network. In the Wavelet Transform (WT) contour plots (Figure 3d−g), the maximum intensity for Co-foil at 7.94 $Å^{-1}$

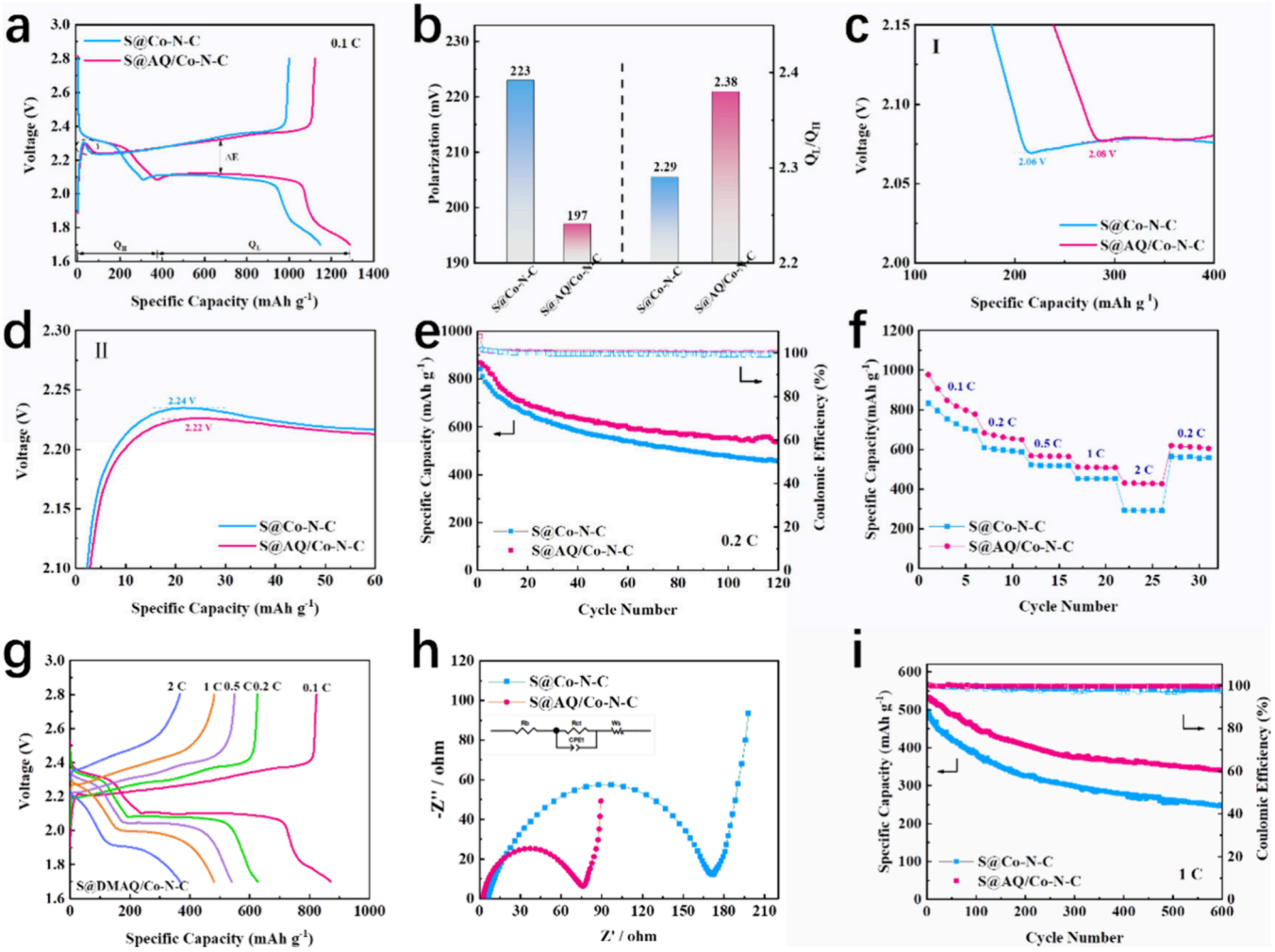

Figure 6. Charging and discharging characteristics of two S@Co−N−C and S@AQ/Co−N−C batteries: (a) Charge−discharge curves for the first cycle at a 0.1 C rate. (b) The calculated values of polarization (ΔE) and Q_L/Q_H. (c) A closer view. (d) Performance at varying rates. (e) Charge−discharge curves of the S@AQ/Co−N−C sample at various current densities. (f) Electrochemical impedance spectroscopy (EIS) of both S@Co−N−C and S@AQ/Co−N−C batteries. (g) Long-cycle performance at a rate of 0.2 C. (h) Long-term cycling tests at 1 C.

is attributed to Co−Co bonds, while the maximum peak for Co−N−C at 8.75 $Å^{-1}$ is due to Co−N bonds. This further validates the Co−N coordination structure. EXAFS fitting results in SI, Table S1, show that the coordination number of the Co−N−C sample is 3.75. These results allow us to conclude that Co atoms in the Co−N−C sample are dispersed in a Co−N_4 structure within the carbon support (Figure 3c), and some Co atoms can also form Co−S bonds with sulfur to facilitate the conversion of polysulfide.

The molecular electrostatic potential (ESP) was employed to identify the potential reactive sites and examine the electrostatic interactions between different molecules.[66] As illustrated in Figure 4a, the AQ molecule exhibits two electrostatic potential minima located near the carbonyl oxygen atoms. This implies that these oxygen atoms are most likely to attract Li ions and form Li−O bonds.[67] To gain a deeper understanding of the interaction between AQ and polysulfides, the two Co−N−C and AQ/Co−N−C samples were immersed separately in a Li_2S_6 solution and allowed to stand for 2 h. After adsorption, the Li_2S_6 solution with the AQ/Co−N−C sample showed significant discoloration, which suggests a strong affinity between AQ/Co−N−C and LiPSs (Figure 4b). The adsorption binding energies shown in Figure 4c suggest that the carbonyl oxygen of AQ adsorbs Li^+ to form Li−O bonds with LiPSs. Theoretically, a compound's redox capability is closely tied to its frontier molecular orbital energy levels. A higher energy level of the highest occupied molecular orbital (HOMO) facilitates a lower electron loss, enabling the compound to function as a reducing agent. Conversely, when the lowest unoccupied molecular orbital (LUMO) lies in a lower energy level, its ability as an oxidizing agent will be enhanced.[68,69] As presented in Figure 4d, the calculated frontier molecular orbital energy levels of Li_2S_x and AQ-Li_2S_x are used to assess the enhancement effect of AQ on the redox kinetics of polysulfides. It is evident that AQ-Li_2S_x has a higher HOMO energy and a lower LUMO energy than Li_2S_x. This implies that AQ-Li_2S_x is more likely to accept electrons as an oxidant during discharge and lose electrons as a reducing agent during charging. In this case, the LUMO and HOMO energies of AQ-Li_2S are −3.22 eV and −4.13 eV, respectively. The higher HOMO energy of AQ-Li_2S (0.14 eV) than that of Li_2S (−4.27 eV) suggests that AQ-Li_2S is more susceptible to oxidation and can more easily convert to Li_2S_4 during the charging process. This theoretical analysis indicates that AQ, by participating in the stabilization of Li_2S_x, can facilitate the

bidirectional conversion of polysulfides and enhance the kinetics of the redox reactions.

To further confirm the effect of the AQ/Co−N−C sample on the catalytic transformation of LiPSs, CV tests were performed to investigate the redox reaction kinetics in Li−S batteries. As depicted in Figure 5a, both electrode samples demonstrate a characteristic two-step redox process. The reduction peak observed at 2.30 V for the S@AQ/Co−N−C sample speaks to the conversion from S_8 to Li_2S_4, and the reduction peak at 2.02 V attributes to the reduction from Li_2S_4 toward insoluble Li_2S_2/Li_2S. The oxidation peaks at 2.34 and 2.42 V correspond to the reverse reactions. In comparison to the S@Co−N−C electrode, the S@AQ/Co−N−C sample exhibits a higher peak current density as well as a smaller peak-to-peak separation of 326 mV, along with a more pronounced splitting between the two oxidation peaks. This indicates that AQ can synergistically work with Co atoms to catalyze the transformation of LiPSs and eventually result in faster reaction kinetics. As demonstrated in SI, Figures S4−S5, the S@AQ/Co−N−C electrode shows smaller Tafel slopes during both the reduction and oxidation processes. This further supports the beneficial effect between AQ and Co−N−C substrate in enhancing the kinetics of the sulfur redox reactions. The Li^+ diffusion rate is also an important indicator in understanding the reaction kinetics of a Li−S battery. For instance, if the kinetics are slow, the cumulative polysulfides in the electrolyte will increase the electrolyte's viscosity. Thus, it is necessary to study the diffusion of Li^+ under different conditions. As illustrated in Figure 5b,c, the Li^+ diffusion coefficient was determined by applying the Randles−Sevick equation, based on the analysis of CV curves obtained at scan rates between 0.1 and 0.5 mV s^{-1}.[68] Figure 5d−f show the peak currents at different potentials and their linear fittings as a function of scan rate. The Li^+ diffusion coefficients, presented in SI, Table S2, were derived from the slopes of the fitted curves. The high diffusion coefficients of Li^+ at different stages for the S@AQ/Co−N−C sample indicate that the battery has rapid redox reaction kinetics. This suggests that AQ effectively promotes the transformation of LiPSs as a redox mediator. To further elucidate the catalytic role of AQ in synergy with Co atoms in the transformation of LiPSs, symmetric cells were employed to assess the conversion kinetics of soluble LiPSs in liquid−liquid phases.[70] As shown in Figure 5g, in the absence of Li_2S_6, the redox current of the electrode is minimal. However, when Li_2S_6 is used as the electrolyte, the symmetric cell assembled with Co−N−C exhibits significant redox peaks. This indicates that evenly distributed Co atoms facilitate the catalytic conversion of the LiPSs. In contrast, the AQ/Co−N−C cell shows more prominent redox peaks and higher peak current densities than the Co−N−C cell. This suggests that the inclusion of AQ enhances the catalytic process of LiPSs by Co−N−C. From a theoretical perspective, the conversion of soluble Li_2S_x to solid Li_2S_2/Li_2S plays a major role in the capacity, and this step governs the rate factor in the whole reduction process.[71] To clearly demonstrate the synergistic effect of the AQ/Co−N−C sample on the catalytic conversion of soluble Li_2S_x to Li_2S, the experiments of constant potential deposition were performed.[36,72] As shown in Figure 5h,i, the prominent current peaks observed for both Co−N−C and AQ/Co−N−C samples suggest efficient Li_2S deposition in each case. The nucleation capacity of Li_2S on the AQ/Co−N−C sample is 511.8 mAh g^{-1}, which is higher than the nucleation capacity of the Co−N−C sample (447.8 mAh g^{-1}). Additionally, the shorter nucleation time signifies a lower LiPSs diffusion and more efficient catalytic conversion. Clearly, AQ/Co−N−C sample exhibits a faster nucleation time of 8098 s than the Co−N−C sample. This indicates that AQ enhances the nucleation, deposition, and catalytic conversion kinetics of Li_2S.

Based on AQ's catalytic transformation of LiPSs and its role in promoting Li_2S dissolution, the advantages of the S@AQ/Co−N−C electrode during the cycling process of Li−S batteries were further evaluated. To isolate the contribution of AQ from the charge and discharge processes, a battery was constructed using lithium foil as the anode and AQ/Co−N−C as the sulfur-free cathode, respectively. As shown in SI, Figure S6, the capacity provided by AQ is minimal and can be considered negligible. Figure 6a shows the initial charge−discharge curves at a rate of 0.1 C for both electrode samples. As seen, the S@AQ/Co−N−C sample exhibits a greater initial discharge capacity of 1290 mAh g^{-1} at 0.1 C compared to that of the S@Co−N−C sample (1155 mAh g^{-1}). Beyond capacity, the voltage distribution (ΔE) also provides valuable insight into the kinetics of the sulfur redox reaction. The S@AQ/Co−N−C sample in Figure 6b exhibits a smaller potential difference of 196 mV. The ratio of low discharge platform capacity (Q_L) to high discharge platform capacity (Q_H) serves as an indicator of the catalyst's effectiveness in promoting the sulfur reduction process. In general, a higher Q_L/Q_H indicates a better catalytic performance.[73] The S@AQ/Co−N−C sample has a higher ratio of 2.68 compared to that of the S@Co−N−C sample (2.43). Figure 6c provides an enlarged view of the starting section of the charging curve from Figure 6a. It can be observed that the S@AQ/Co−N−C sample exhibits a lower Li_2S activation potential (2.22 V). More specifically, this indicates that Li_2S has a lower decomposition energy barrier on AQ/Co−N−C sample, which makes it easier to convert to active sulfur.[74] Additionally, Figure 6d illustrates the rate performance of two samples at current densities ranging between 0.1 and 2 C. The S@AQ/Co−N−C sample demonstrates discharge capacities of 977, 683, 568, 511, and 431 mAh g^{-1} at 0.1, 0.2, 0.5, 1, and 2 C, respectively. Upon the current density returning to 0.2 C, the discharge capacity stays at 619 mAh g^{-1}, and this translates to a 91% capacity retention. The charge−discharge curves for the S@AQ/Co−N−C sample at various current densities are illustrated in Figure 6e. It is observed that as the current density increases polarization becomes more pronounced. This suggests that the higher current densities slow the reaction kinetics and increase the internal resistance of the battery. Notably, the characteristic discharge plateau of Li−S batteries is retained by the S@AQ/Co−N−C sample, even at higher current densities. Compared to S@Co−N−C electrode sample shown in SI, Figure S7, S@AQ/Co−N−C sample exhibits a lower polarization and demonstrates a significant positive synergistic effect between AQ and Co−N−C substrate in promoting sulfur redox reactions. To further confirm the benefits of the S@AQ/Co−N−C electrode in improving reaction kinetics, electrochemical impedance spectroscopy (EIS) was evaluated on both S@Co−N−C and S@AQ/Co−N−C batteries. As observed, the spectra in Figure 6f feature a low-frequency sloped line and a high-frequency semicircle, which representing the ion diffusion process and charge transfer process, respectively.[75] The S@AQ/Co−N−C sample demonstrates lower charge transfer resistance and ion diffusion resistance compared with the S@Co−N−C sample. This further indicates a positive

synergistic effect of AQ and Co−N−C in promoting the transformation of the LiPSs. To assess the superior cycling stability of S@AQ/Co−N−C electrode, long-term cycling tests were conducted on two S@Co−N−C and S@AQ/Co−N−C samples at a rate of 0.2 C. As shown in Figure 6g, the S@AQ/Co−N−C electrode exhibits an initial discharge capacity of 868 mAh g^{-1} at 0.2 C, and maintains 62% capacity retention after 120 cycles. This underscores the significant role of AQ in improving the cycling stability of the Li−S batteries. Additionally, the long-cycle performance of the S@AQ/Co−N−C electrode at 1 C was evaluated in Figure 6h, in which a discharge capacity of 338 mAh g^{-1} after 600 cycles corresponds to a cycle-to-cycle decay rate of just 0.06%. Compared with other studies in the literature, the S@AQ/Co−N−C electrode demonstrates outstanding cycle stability for Li−S batteries (SI, Table S3). Furthermore, as depicted in SI, Figure S8, the cycling stability of the S@AQ/Co−N−C sample was assessed at sulfur loadings of 3.5 mg cm^{-2} with an E/S ratio of 8 μL mg^{-1} and 5.0 mg cm^{-2} with an E/S ratio of 6 μL mg^{-1} at 0.2 C. The initial discharge capacities were 521 mAh g^{-1} and 427 mAh g^{-1}, respectively. After 100 cycles, the capacity retention rates were 71% and 65%, with corresponding cycle decay rates of only 0.29% and 0.35%, respectively. The S@AQ/Co−N−C electrode exhibits both high discharge capacity and excellent cycling stability even under high sulfur loading, highlighting the strong positive synergistic effect between AQ and Co−N−C. These results clearly demonstrate that AQ, as a redox mediator, accelerates the polysulfide redox reaction kinetics, improves sulfur utilization, and exhibits a robust synergy with Co−N−C in enhancing overall performance.

4. CONCLUSION

This study demonstrates the effective dual-function regulation of LiPSs and Li_2S conversion using anthraquinone (AQ) as a redox mediator combined with Co atoms. The findings reveal that AQ plays a key role in lowering the reaction barrier of Li_2S, promoting the conversion of the insulating Li_2S to LiPSs, providing an additional redox pathway, enhancing the reversibility of active sulfur species, and reactivating "dead sulfur." Moreover, Co atoms catalyze the transformation of LiPSs and reduce unwanted side reactions between LiPSs and the lithium anode. The synergistic effect of AQ and Co efficiently governs the bidirectional conversion between Li_2S and LiPSs. Thanks to these attributes, the S@AQ/Co−N−C electrode demonstrates superior performance across a range of rates (0.1 0.2, 0.5, 1, and 2 C), and achieves a remarkable 91% capacity retention when the current density restored to 0.2 C. The initial discharge capacity at 0.1 C reaches 1290 mAh g^{-1}, and at 1 C, the capacity decay rate remains low at 0.06% per cycle after 600 cycles. These findings suggest the potential to achieve high-performance Li−S batteries by efficiently regulating the bidirectional conversion of LiPSs under practical operating conditions.

ASSOCIATED CONTENT

Supporting Information

The Supporting Information is available free of charge at https://pubs.acs.org/doi/10.1021/acsami.4c13898.

Materials characterization results, including UV−visible absorption and a performance comparison (PDF)

AUTHOR INFORMATION

Corresponding Authors

Rongfang Wang − *College of Chemical Engineering, Qingdao University of Science and Technology, Qingdao 266042, China*; orcid.org/0000-0001-9055-7408; Email: rfwang@qust.edu.cn

Xuyun Wang − *College of Chemical Engineering, Qingdao University of Science and Technology, Qingdao 266042, China*; Email: wangxy@qust.edu.cn

Jianwei Ren − *Department of Chemical Engineering, University of Pretoria, Hatfield 0028, South Africa*; Email: jianwei.ren@up.ac.za

Authors

Huijuan You − *College of Chemical Engineering, Qingdao University of Science and Technology, Qingdao 266042, China*

Zining Wang − *School of Chemical Science and Engineer, Tongji University, Shanghai 200092, China*; orcid.org/0000-0002-6691-8258

Hui Wang − *College of Chemical Engineering, Qingdao University of Science and Technology, Qingdao 266042, China*

Complete contact information is available at: https://pubs.acs.org/10.1021/acsami.4c13898

Author Contributions

H.Y. and Z.W. made equal contributions to this work. H.Y. conducted the experiments, collected the data, and drafted the first manuscript. Z.W. performed the in situ synchrotron radiation testing and analysis. J.R. and H.W. contributed to the writing and revision. X.W. and R.W. provided financial support for this work.

Notes

The authors declare no competing financial interest.

ACKNOWLEDGMENTS

We gratefully acknowledge the financial support provided by the Open Project Program (no. EFMD2021001Z) of the Guangdong Provincial Key Laboratory for Electronic Functional Materials and Devices from Huizhou University, China.

REFERENCES

(1) Goodenough, J. B.; Kim, Y. Challenges for Rechargeable Li Batteries. *Chem. Mater.* **2010**, *22* (3), 587−603.

(2) Armand, M.; Tarascon, J. M. Building better batteries. *Nature* **2008**, *451* (7179), 652−657.

(3) Chung, S. H.; Manthiram, A. Current Status and Future Prospects of Metal-Sulfur Batteries. *Adv. Mater.* **2019**, *31* (27), 1901125.

(4) Zhou, G.; Chen, H.; Cui, Y. Formulating energy density for designing practical lithium-sulfur batteries. *Nat. Energy.* **2022**, *7* (4), 312−319.

(5) Wang, L.; Wu, Z.; Zou, J.; Gao, P.; Niu, X.; Li, H.; Chen, L. Li-free Cathode Materials for High Energy Density Lithium Batteries. *Joule* **2019**, *3* (9), 2086−2102.

(6) Liu, X.; Li, Y.; Xu, X.; Zhou, L.; Mai, L. Rechargeable metal (Li, Na, Mg, Al)-sulfur batteries: Materials and advances. *J. Energy Chem.* **2021**, *61*, 104−134.

(7) Gao, X.; Yang, H. Multi-electron reaction materials for high energy density batteries. *Energ Environ. Sci.* **2010**, *3* (2), 174−189.

(8) Seh, Z. W.; Sun, Y.; Zhang, Q.; Cui, Y. Designing high-energy lithium-sulfur batteries. *Chem. Soc. Rev.* **2016**, *45* (20), 5605−5634.

(9) Wild, M.; O'Neill, L.; Zhang, T.; Purkayastha, R.; Minton, G.; Marinescu, M.; Offer, G. J. Lithium sulfur batteries, a mechanistic review. *Energ Environ. Sci.* **2015**, *8* (12), 3477−3494.
(10) Deng, C.; Wang, Z.; Wang, S.; Yu, J. Inhibition of polysulfide diffusion in lithium-sulfur batteries: mechanism and improvement strategies. *J. Mater. Chem. A* **2019**, *7* (20), 12381−12413.
(11) Li, H.; Ma, S.; Li, J.; Liu, F.; Zhou, H.; Huang, Z.; Jiao, S.; Kuang, Y. Altering the reaction mechanism to eliminate the shuttle effect in lithium-sulfur batteries. *Energy Storage Mater.* **2020**, *26*, 203−212.
(12) Zhang, Z.; Kong, L.; Liu, S.; Li, G.; Gao, X. A High-Efficiency Sulfur/Carbon Composite Based on 3D Graphene Nanosheet@ Carbon Nanotube Matrix as Cathode for Lithium-Sulfur Battery. *Adv. Energy Mater.* **2017**, *7* (11), 1602543.
(13) Lin, D.; Liu, Y.; Cui, Y. Reviving the lithium metal anode for high-energy batteries. *Nat. Nanotechnol.* **2017**, *12* (3), 194−206.
(14) Tu, S.; Chen, X.; Zhao, X.; Cheng, M.; Xiong, P.; He, Y.; Zhang, Q.; Xu, Y. A Polysulfide-Immobilizing Polymer Retards the Shuttling of Polysulfide Intermediates in Lithium-Sulfur Batteries. *Adv. Mater.* **2018**, *30* (45), 1804581.
(15) Li, G.; Li, G.; Ye, S.; Gao, X. A Polyaniline-Coated Sulfur/Carbon Composite with an Enhanced High-Rate Capability as a Cathode Material for Lithium/Sulfur Batteries. *Adv. Energy Mater.* **2012**, *2* (10), 1238−1245.
(16) Zhang, L.; Liu, D.; Muhammad, Z.; Wan, F.; Xie, W.; Wang, Y.; Song, L.; Niu, Z.; Chen, J. Single Nickel Atoms on Nitrogen-Doped Graphene Enabling Enhanced Kinetics of Lithium-Sulfur Batteries. *Adv. Mater.* **2019**, *31* (40), 1903955.
(17) Huang, J.; Zhuang, T.; Zhang, Q.; Peng, H.; Chen, C.; Wei, F. Permselective Graphene Oxide Membrane for Highly Stable and Anti-Self-Discharge Lithium-Sulfur Batteries. *ACS Nano* **2015**, *9* (3), 3002−3011.
(18) Bai, S.; Liu, X.; Zhu, K.; Wu, S.; Zhou, H. Metal-organic framework-based separator for lithium-sulfur batteries. *Nat. Energy.* **2016**, *1*, 16094.
(19) Pan, J.; Shi, K.; Sun, Y.; Wu, Y.; Li, J.; Li, K.; Wu, H.; Wang, Z.; Dong, H.; Liu, Q. Activating redox kinetics of polysulfides within edge-rich nitrogen doped porous interconnected carbon nanosphere. *Chem. Eng. Sci.* **2023**, *274*, 118640−118652.
(20) Xie, J.; Peng, H.; Huang, J.; Xu, W.; Chen, X.; Zhang, Q. A Supramolecular Capsule for Reversible Polysulfide Storage/Delivery in Lithium-Sulfur Batteries. *Angew. Chem., Int. Ed.* **2017**, *56* (51), 16223−16227.
(21) Liao, H.; Wang, H.; Ding, H.; Meng, X.; Xu, H.; Wang, B.; Ai, X.; Wang, C. A 2D porous porphyrin-based covalent organic framework for sulfur storage in lithium sulfur batteries. *J. Mater. Chem. A* **2016**, *4* (19), 7416−7421.
(22) Chung, S.; Manthiram, A. Carbonized Eggshell Membrane as a Natural Polysulfide Reservoir for Highly Reversible Li-S Batteries. *Adv. Mater.* **2014**, *26* (9), 1360−1365.
(23) Hua, W.; Yang, Z.; Nie, H.; Li, Z.; Yang, J.; Guo, Z.; Ruan, C.; Chen, X.; Huang, S. Polysulfide-Scission Reagents for the Suppression of the Shuttle Effect in Lithium-Sulfur Batteries. *ACS Nano* **2017**, *11* (2), 2209−2218.
(24) Yang, T.; Qian, T.; Liu, J.; Xu, N.; Li, Y.; Grundish, N.; Yan, C.; Goodenough, J. B. A New Type of Electrolyte System To Suppress Polysulfide Dissolution for Lithium Sulfur Battery. *ACS Nano* **2019**, *13* (8), 9067−9073.
(25) Lei, J.; Liu, T.; Chen, J.; Zheng, M.; Zhang, Q.; Mao, B.; Dong, Q. Exploring and Understanding the Roles of Li_2S_n and the Strategies to beyond Present Li-S Batteries. *Chem.* **2020**, *6* (10), 2533−2557.
(26) Wang, Y.; Huang, X.; Zhang, S.; Hou, Y. Sulfur Hosts against the Shuttle Effect. *Small Methods* **2018**, *2* (6), 1700345.
(27) Ng, S. F.; Lau, M.; Ong, W. J. Lithium-Sulfur Battery Cathode Design: Tailoring Metal-Based Nanostructures for Robust Polysulfide Adsorption and Catalytic Conversion. *Adv. Mater.* **2021**, *33* (50), 2008654.
(28) Wang, P.; Xi, B.; Huang, M.; Chen, W.; Feng, J.; Xiong, S. Emerging Catalysts to Promote Kinetics of Lithium-Sulfur Batteries. *Adv. Energy Mater.* **2021**, *11* (7), 2002893.
(29) Zhang, J.; Huang, H.; Bae, J.; Chung, S.; Zhang, W.; Manthiram, A.; Yu, G. Nanostructured Host Materials for Trapping Sulfur in Rechargeable Li-S Batteries: Structure Design and Interfacial Chemistry. *Small Methods* **2018**, *2*, 1700279.
(30) Kong, L.; Chen, J.; Peng, H.; Huang, J.; Zhu, W.; Jin, Q.; Li, B.; Zhang, X.; Zhang, Q. Current-density dependence of Li_2S/Li_2S_2 growth in lithium-sulfur batteries. *Energ Environ. Sci.* **2019**, *12* (10), 2976−2982.
(31) Feng, S.; Fu, Z.; Chen, X.; Zhang, Q. A review on theoretical models for lithium-sulfur battery cathodes. *Infomat* **2022**, *4*, 12304.
(32) Chen, Z.; Lv, W.; Kang, F.; Li, J. Theoretical Investigation of the Electrochemical Performance of Transition Metal Nitrides for Lithium−Sulfur Batteries. *J. Phys. Chem. C* **2019**, *123* (41), 25025−25030.
(33) Yang, J.; Cai, D.; Lin, Q.; Wang, X.; Fang, Z.; Huang, L.; Wang, Z.; Hao, X.; Zhao, S.; Li, J.; Cao, G.; Lv, W. Regulating the Li_2S deposition by grain boundaries in metal nitrides for stable lithium-sulfur batteries. *Nano Energy* **2022**, *91*, 106669.
(34) Deng, S.; Guo, T.; Heier, J.; Zhang, C. Unraveling Polysulfide's Adsorption and Electrocatalytic Conversion on Metal Oxides for Li-S Batteries. *Adv. Sci.* **2023**, *10* (5), 2204930.
(35) Xiao, W.; Kiran, G.; Yoo, K.; Kim, J. H.; Xu, H. The Dual-Site Adsorption and High Redox Activity Enabled by Hybrid Organic-Inorganic Vanadyl Ethylene Glycolate for High-Rate and Long-Durability Lithium−Sulfur Batteries. *Small* **2023**, *19* (20), 2206750.
(36) Liu, F.; Luo, W.; Zhang, Z.; Yu, J.; Cai, J.; Yang, Z. Cation-doped V_2O_5 microsphere as a bidirectional catalyst to activate sulfur redox reactions for lithium-sulfur batteries. *Chem. Eng. J.* **2023**, *456*, 140948.
(37) Li, J.; Wang, Z.; Shi, K.; Wu, Y.; Huang, W.; Min, Y.; Liu, Q.; Liang, Z. Nanoreactors Encapsulating Built-in Electric Field as a "Bridge" for Li−S Batteries: Directional Migration and Rapid Conversion of Polysulfides. *Adv. Energy Mater.* **2024**, *14* (9), 2303546.
(38) Liu, F.; Wang, N.; Shi, C.; Sha, J.; Ma, L.; Liu, E.; Zhao, N. Phosphorus doping of 3D structural MoS_2 to promote catalytic activity for lithium-sulfur batteries. *Chem. Eng. J.* **2022**, *431*, 133923.
(39) Ai, G.; Hu, Q.; Zhang, L.; Dai, K.; Wang, J.; Xu, Z.; Huang, Y.; Zhang, B.; Li, D.; Zhang, T.; Liu, G.; Mao, W. Investigation of the Nanocrystal CoS_2 Embedded in 3D Honeycomb-like Graphitic Carbon with a Synergistic Effect for High-Performance Lithium Sulfur Batteries. *ACS Appl. Mater.* **2019**, *11* (37), 33987−33999.
(40) Li, T.; Sun, Y.; Shi, K.; Qin, W.; Chen, H.; Li, J.; Zheng, Y.; Liu, Q.; Liang, Z. The d-band energy level splitting of ferric group (Fe, Co, Ni) metals drives the adsorption-conversion of polysulfides. *AIChE J.* **2024**, *70* (3), e18327.
(41) Zhao, Z.; Zhang, X.; Zhou, Z.; Wang, E.; Peng, Z. Direct In Situ Spectroscopic Evidence for Solution-Mediated Oxygen Reduction Reaction Intermediates in Aprotic Lithium−Oxygen Batteries. *Nano Lett.* **2022**, *22* (1), 501−507.
(42) Wu, S.; Yang, J.; Qin, N.; Li, Y.; Wang, H.; Zhang, Y.; Wang, Q.; Lu, Z. Ethyl Viologen as a Superoxide Quencher to Enhance the Oxygen Reduction Reaction in Li−O_2 Batteries. *ACS Appl. Energy Mater.* **2022**, *5* (7), 9040−9048.
(43) Wu, S.; Qin, N.; Zhang, H.; Wei, C.; Wang, Z.; Luo, W.; Li, Y.; Wang, H.; Zhang, K.; Wang, Q.; Lu, Z. Revealing the catalytic pathway of a quinone-mediated oxygen reduction reaction in aprotic Li−O_2 batteries. *Chem. Commun.* **2022**, *58* (7), 1025−1028.
(44) Zhu, L.; Ding, G.; Han, Q.; Miao, Y.; Li, X.; Yang, X.; Chen, L.; Wang, G.; Xie, L.; Cao, X. Enhancing electrochemical performances of small quinone toward lithium and sodium energy storage. *Rare Metals* **2022**, *41* (2), 425−437.
(45) Gao, R.; Ji, S.; Wang, K.; Linkov, V.; Ma, X.; Wang, H. 2,6-dimethoxy anthraquinone as redox mediator for the reversible deposition-dissolution of Li_2S in lithium-sulfur batteries. *Chem. Eng. J.* **2024**, *484*, 149611−149620.

(46) Zheng, Q.; Fan, X.; Liu, G.; Hou, Q.; Fan, J.; Zheng, M.; Dong, Q. Enhancing sulfur cathode process via a functionalized complex molecule. *Nano Res.* **2023**, *16* (6), 8385−8393.
(47) Lai, T.; Manthiram, A. Phloroglucinol−2,6-Diaminoanthraquinone as a Durable Redox Mediator for Enhancing Conversion Reaction Kinetics in Lithium-Sulfur Batteries. *Adv. Funct. Mater.* **2024**, *34*, 2405814.
(48) Gao, X.; Zheng, X.; Tsao, Y.; Zhang, P.; Xiao, X.; Ye, Y.; Li, J.; Yang, Y.; Xu, R.; Bao, Z.; Cui, Y. All-Solid-State Lithium-Sulfur Batteries Enhanced by Redox Mediators. *J. Am. Chem. Soc.* **2021**, *143* (43), 18188−18195.
(49) Peng, Y.; Zhao, M.; Chen, Z.; Cheng, Q.; Liu, Y.; Li, X.; Song, Y.; Li, B.; Huang, J. Boosting sulfur redox kinetics by a pentacenetetrone redox mediator for high-energy-density lithium-sulfur batteries. *Nano Res.* **2023**, *16* (6), 8253−8259.
(50) Zhang, W.; Ma, F.; Wu, Q.; Cai, Z.; Zhong, W.; Zeng, Z.; Cheng, S.; Xie, J. Bifunctional Fluorinated Anthraquinone Additive for Improving Kinetics and Interfacial Chemistry in Rechargeable Li-S Batteries. *ACS Appl. Energy Mater.* **2022**, *5* (12), 15719−15728.
(51) Tamirat, A. G.; Guan, X.; Liu, J.; Luo, J.; Xia, Y. Redox mediators as charge agents for changing electrochemical reactions. *Chem. Soc. Rev.* **2020**, *49* (20), 7454−7478.
(52) Zhang, L.; Zhang, Z.; Wu, H.; Amine, K. Novel redox shuttle additive for high-voltage cathode materials. *Energ Environ. Sci.* **2011**, *4* (8), 2858−2862.
(53) Bruce, P. G.; Freunberger, S. A.; Hardwick, L. J.; Tarascon, J. M. Li-O_2 and Li-S batteries with high energy storage. *Nat. Mater.* **2012**, *11* (1), 19−29.
(54) Lim, H. D.; Lee, B.; Zheng, Y.; Hong, J.; Kim, J.; Gwon, H.; Ko, Y.; Lee, M.; Cho, K.; Kang, K. Rational design of redox mediators for advanced Li−O_2 batteries. *Nat. Energy.* **2016**, *1*, 16066.
(55) Leverick, G.; Tulodziecki, M.; Tatara, R.; Barde, F.; Yang, S.-H. Solvent-Dependent Oxidizing Power of LiI Redox Couples for Li-O_2 Batteries. *Joule* **2019**, *3* (4), 1106.
(56) Tsao, Y.; Lee, M.; Miller, E. C.; Gao, G.; Park, J.; Chen, S.; Katsumata, T.; Tran, H.; Wang, L.; Toney, M. F.; Cui, Y.; Bao, Z. Designing a Quinone-Based Redox Mediator to Facilitate Li_2S Oxidation in Li-S Batteries. *Joule* **2019**, *3* (3), 872−884.
(57) Peng, H. J.; Zhang, G.; Chen, X.; Zhang, X.; Xu, W.; Huang, J.; Zhang, Q. Enhanced Electrochemical Kinetics on Conductive Polar Mediators for Lithium-Sulfur Batteries. *Angew. Chem., Int. Ed. Engl.* **2016**, *55* (42), 12990−12995.
(58) Li, G.; Wang, X.; Seo, M. H.; Li, M.; Ma, L.; Yuan, Y.; Wu, T.; Yu, A.; Wang, S.; Lu, J.; Chen, Z. Chemisorption of polysulfides through redox reactions with organic molecules for lithium-sulfur batteries. *Nat. Commun.* **2018**, *9*, 705.
(59) Xie, J.; Peng, H.; Song, Y.; Li, B.; Xiao, Y.; Zhao, M.; Yuan, H.; Huang, J.; Zhang, Q. Spatial and Kinetic Regulation of Sulfur Electrochemistry on Semi-Immobilized Redox Mediators in Working Batteries. *Angew. Chem., Int. Ed. Engl.* **2020**, *59* (40), 17670−17675.
(60) Zhang, F.; Ji, S.; Wang, H.; Liang, H.; Wang, X.; Wang, R. Implanting Cobalt Atom Clusters within Nitrogen-Doped Carbon Network as Highly Stable Cathode for Lithium-Sulfur Batteries. *Small Methods* **2021**, *5*, 2100066.
(61) Yang, J.; Wang, Z.; Shi, Y.; Sun, P.; Xu, Y. Poorly Soluble 2,6-Dimethoxy-9,10-anthraquinone Cathode for Lithium-Ion Batteries: The Role of Electrolyte Concentration. *ACS Appl. Mater.* **2020**, *12* (6), 7179−7185.
(62) Wang, P.; Zeng, R.; You, L.; Tang, H.; Zhong, J.; Wang, S.; Yang, T.; Liu, J. Graphene-Like Matrix Composites with Fe_2O_3 and Co_3O_4 as Cathode Materials for Lithium-Sulfur Batteries. *ACS Appl. Nano Mater.* **2020**, *3* (2), 1382−1390.
(63) Wang, L.; Guan, E.; Wang, Y.; Wang, L.; Gong, Z.; Cui, Y.; Meng, X.; Gates, B. C.; Xiao, F. Silica accelerates the selective hydrogenation of CO_2 to methanol on cobalt catalysts. *Nat. Commun.* **2020**, *11*, 1722.
(64) Fang, S.; Zhu, X.; Liu, X.; Gu, J.; Liu, W.; Wang, D.; Zhang, W.; Lin, Y.; Lu, J.; Wei, S.; Li, Y.; Yao, T. Uncovering near-free platinum single-atom dynamics during electrochemical hydrogen evolution reaction. *Nat. Commun.* **2020**, *11*, 1029.
(65) Wei, S.; Zhang, P.; Xu, W.; Chen, S.; Xia, Y.; Cao, Y.; Zhu, K.; Cui, Q.; Wen, W.; Wu, C.; Wang, C.; Song, L. Operando Exploring and Modulating Phase Evolution Chemistry from MAX to MXenes in Molten Salt Synthesis. *J. Am. Chem. Soc.* **2023**, *145* (19), 10681−10690.
(66) Lu, T.; Chen, F. Multiwfn: A multifunctional wavefunction analyzer. *J. Comput. Chem.* **2012**, *33* (5), 580−592.
(67) Gao, R.; Wang, K.; Wang, F.; Wang, H.; Wang, X.; Ren, J.; Wang, R. Synthetic perylenequinone as anchoring center of sulfur and catalyst for polysulfides conversion. *Chem. Eng. J.* **2023**, *455*, 140847.
(68) Rui, X.; Ding, N.; Liu, J.; Li, C.; Chen, C. Analysis of the chemical diffusion coefficient of lithium ions in $Li_3V_2(PO_4)_3$ cathode material. *Electrochim. Acta* **2010**, *55* (7), 2384−2390.
(69) Yang, J.; Xiong, P.; Shi, Y.; Sun, P.; Wang, Z.; Chen, Z.; Xu, Y. Rational Molecular Design of Benzoquinone-Derived Cathode Materials for High-Performance Lithium-Ion Batteries. *Adv. Funct Mater.* **2020**, *30*, 1909597.
(70) Qiu, W.; Li, G.; Luo, D.; Zhang, Y.; Zhao, Y.; Zhou, G.; Shui, L.; Wang, X.; Chen, Z. Hierarchical Micro-Nanoclusters of Bimetallic Layered Hydroxide Polyhedrons as Advanced Sulfur Reservoir for High-Performance Lithium-Sulfur Batteries. *Adv. Sci.* **2021**, *8* (7), 2003400.
(71) Kong, Z.; Liu, Q.; Liu, X.; Wang, Y.; Shen, C.; Zhan, L. Co-N_x bonds as bifunctional electrocatalytic sites to drive the reversible conversion of lithium polysulfides for long life lithium sulfur batteries. *Appl. Surf. Sci.* **2021**, *546*, 148914−148925.
(72) Chu, R.; Nguyen, T. T.; Bai, Y.; Kim, N. H.; Lee, J. H. Uniformly Controlled Treble Boundary Using Enriched Adsorption Sites and Accelerated Catalyst Cathode for Robust Lithium-Sulfur Batteries. *Adv. Energy Mater.* **2022**, *12*, 2102805.
(73) Xu, J.; Xu, L.; Zhang, Z.; Sun, B.; Jin, Y.; Jin, Q.; Liu, H.; Wang, G. Heterostructure ZnSe-$CoSe_2$ embedded with yolk-shell conductive dodecahedral as Two-in-one hosts for cathode and anode protection of Lithium-Sulfur full batteries. *Energy Storage Mater.* **2022**, *47*, 223−234.
(74) Lefebvre, C.; Rubez, G.; Khartabil, H.; Boisson, J. C.; Contreras-Garcia, J.; Henon, E. Accurately extracting the signature of intermolecular interactions present in the NCI plot of the reduced density gradient versus electron density. *PCCP.* **2017**, *19*, 17928.
(75) Pan, J.; Sun, Y.; Wu, Y.; Li, J.; Huang, W.; Shi, K.; Lin, Y.; Dong, H.; Liu, Q. Yolk-double shells hierarchical N-doped carbon nanosphere as an electrochemical nanoreactor for high performance lithium-sulfur batteries. *Carbon* **2022**, *198*, 80−90.